Effect of different parameters on grinding efficiency and its monitoring by acoustic emission

Xun Chen and Tahsin T. Öpöz

General Engineering Research Institute

Liverpool John Moores University, Liverpool L3 3AF, UK

x.chen@ljmu.ac.uk

Biographical notes:

X. Chen is currently a professor of manufacturing in Liverpool John Moores University. He has previously been an academic in the University of Huddersfield, the University of Nottingham, the University of Dundee and Fuzhou University and a royal research fellow in Liverpool Polytechnic. He specialises in advanced manufacturing technology including application of computing science, mechatronics and artificial intelligence to manufacturing process monitoring, control and optimisation, particularly to abrasive machining technology. He obtained his BEng from Fuzhou University, MSc from Zhejiang University and PhD from Liverpool John Moores University.

T. T. Öpöz is currently a senior lecturer in Liverpool John Moores University. He received his BSc degree in Mechanical Engineering from Gaziantep University, MSc degree in Mechatronics Engineering from Atilim University, PhD from Huddersfield University. He specialises in advanced manufacturing technologies including precision grinding, modelling and simulation of machining processes, and Electrical Discharge Machining.

Effect of different parameters on grinding efficiency and its monitoring by acoustic emission

Abstract

Grinding efficiency is one of the most important considerations in the selection of grinding operation conditions because it has a significant impact on the productivity, quality, energy consumption and cost of production. Focusing on the core issues of grinding process, the paper presents some fundamental research findings in relation to grinding material removal mechanisms. The grinding efficiency is analysed by considering the rubbing, ploughing and cutting three stages of a single grit grinding process. By analysing the features of acoustic emission in single grit grinding tests, an evidence based scientific foundation has been established for monitoring grinding efficiency using acoustic emission. Accordingly, the energy consumption in the grinding is considered with the grit shape. Following the discussion of the models of temperature elevation and thermal stresses in grinding, the paper provides a logic depiction that explains why acoustic emission in grinding can be used for grinding thermal performance monitoring. As a result, the paper introduces a novel acoustic emission monitoring method that is capable to monitor grinding temperature and grinding wheel wear status.

Keywords: Grinding efficiency, Single grit grinding, Temperature, Acoustic emission, Neural network.

Introduction

Grinding operation is commonly applied to material removal in order to achieve required size and form accuracy with specified surface finish. It is commonly considered to be a final material removing process, so its quality has direct influence on the component functional performance. Today grinding process has been successfully applied to almost all types of material removing process with extremely high material removal rate of more than 2000 $mm^3/(mm\ s)$ and ultra-precision accuracy to nanometre lever surface finish (Comley, Walton, Jin, & Stephenson, 2006; Zhou, 2010). Due to the high hardness of abrasives used as cutting media, grinding is often the first choice for removing materials of high hardness. The application of grinding possesses more than a quarter of total machining processes and is still increasing (Chen, 2009). Wide use of grinding process becomes an important feature of manufacturing process in modern industry. To fully understand grinding mechanism of material removal and associated grinding phenomena is critical to provide guidance for further improving grinding quality and productivity.

During grinding, rich acoustic emission (AE) signals emit from grinding zone because high stress and strain are associated with the material removal. Therefore AE signals can play an important role in grinding process monitoring. The advantage of AE sensor is easy to mount and works at relatively low cost. There is no negative influence on the stiffness of the machine tools and is even capable of transmitting a signal from its rotating parts. The AE sensor has much higher sensitivity and responsive

speed compare to force or power sensors because the AE phenomenon is related to the elastic energy release at a very high frequency range. By monitoring grinding AE signals in relation to the variation of grinding material removal mechanism, it is possible to indicate the grinding efficiency changes and associated grinding phenomena (Chen, Griffin, & Liu, 2007; Han & Wu, 2013; Griffin & Chen. 2014). Recent research (Batako & Goh, 2014) has demonstrated the AE signals can well represent the dynamic performance of a grinding system in relation to material removal and workpiece surface formation, where the features of workpiece roundness can be identified from AE signals.

This paper focuses on the fundamental of material removal in grinding and associated acoustic emission (AE) phenomenon to illustrate some interesting relationships between grinding AE features and the grinding mechanical and thermal performance. As the stress exists in the grinding zone is the key source of grinding acoustic emission, models are developed to present grinding force, temperature and associated stress level in relation to the grinding controllable parameters. The paper further demonstrates a novel method for grinding process monitoring using a neural network based on the identified grinding mechanism and relations.

Fundamentals of grinding mechanism

As a materials removal process, grinding process is similar to other cutting processes in many respects, such as materials are removed in forms of chips (Rowe, 2009; Chen, 2009). However grinding has its distinctness from other machining processes. Firstly, abrasive grits on the wheel surface are of irregular shapes and are randomly positioned. Therefore statistical analysis is commonly used in the investigation of grinding. Secondly, the undeformed cutting depth of each grit or cutting edge in grinding is very thin, down to sub micrometre or nanometre level. The cutting chip may not form in each grit pass in the grinding zone. Thirdly, grinding cutting speed is much higher than other machining process. Normally it is 10 times higher. High grinding speed provides the increase of materials removal rate, but it also introduces the problem of high grinding temperature. A special feature in grinding has to be mentioned is the self-sharpening action of grinding wheel. When a cutting tool is worn or damaged during machining process, it requires replacing by new one or re-sharpening. However the wear of an individual grit on the surface of grinding wheel may not make a large effect on the grinding wheel performance. Such wear may increase the force on the worn grit so as to fracture the grit itself creating new sharp cutting edges or to force the worn grit dropped off from the wheel surface allowing new grits in the lower layer of the wheel engaging in the grinding process. Because of the self-sharpening action, grinding wheel is able to grind materials of similar hardness to the abrasive grits.

Considering such distinct features of grinding, systematic consideration is required in practice (Chen, & Rowe, 1996; Chen, Rowe, & Cai, 2002). The systematic consideration of a grinding process requires the knowledge of inputs and outputs of the grinding process. In fact a grinding process is a material removal process utilising a grinding wheel, which is made of a large number of randomly positioned grits. Following the grinding kinematic paths, the grits on the wheel surface successively penetrate the workpiece to remove the material in front of their paths. Focussing on grit and workpiece interactions, the relationship between influential parameters and grinding performance can be summarised as in Fig. 1. The factors on the top layer are the primary inputs to a grinding process and the outputs are presented at the bottom. The grinding environment includes the atmosphere, coolant delivery and the machine structure that holds the wheel and workpiece at a correct position.

The grinding system behaviour is primarily considered from the viewpoints of geometry, kinematics, mechanics, energy consumption, thermal behaviours and material performance. The performance of a grinding operation is usually assessed by using force, vibration, temperature, ground surface integrity and roundness. A good grinding with well-dressed wheel presents low force and temperature, consistent accuracy, satisfactory workpiece surface integrity and roughness. Large variations of grinding behaviour are not acceptable.

Actual grinding performance can be considered as the summation of the performance of individual grits (Chen, & Rowe, 1996). Based on the relationships illustrated in Fig. 1, improvement and stabilisation of grinding performance may be achieved by considering grinding wheel surface topography, chip formation and materials properties as well as grinding environment including machine structure, coolant delivery, and so on. It can be seen that the inputs and outputs of a grinding process is linked by the work load on individual grit in the grinding wheel. Understanding a grinding process starts from the material removal of individual grit actions. Therefore the core issue of grinding performance should be the single grit load. The grinding efficiency is determined by each individual grit load.

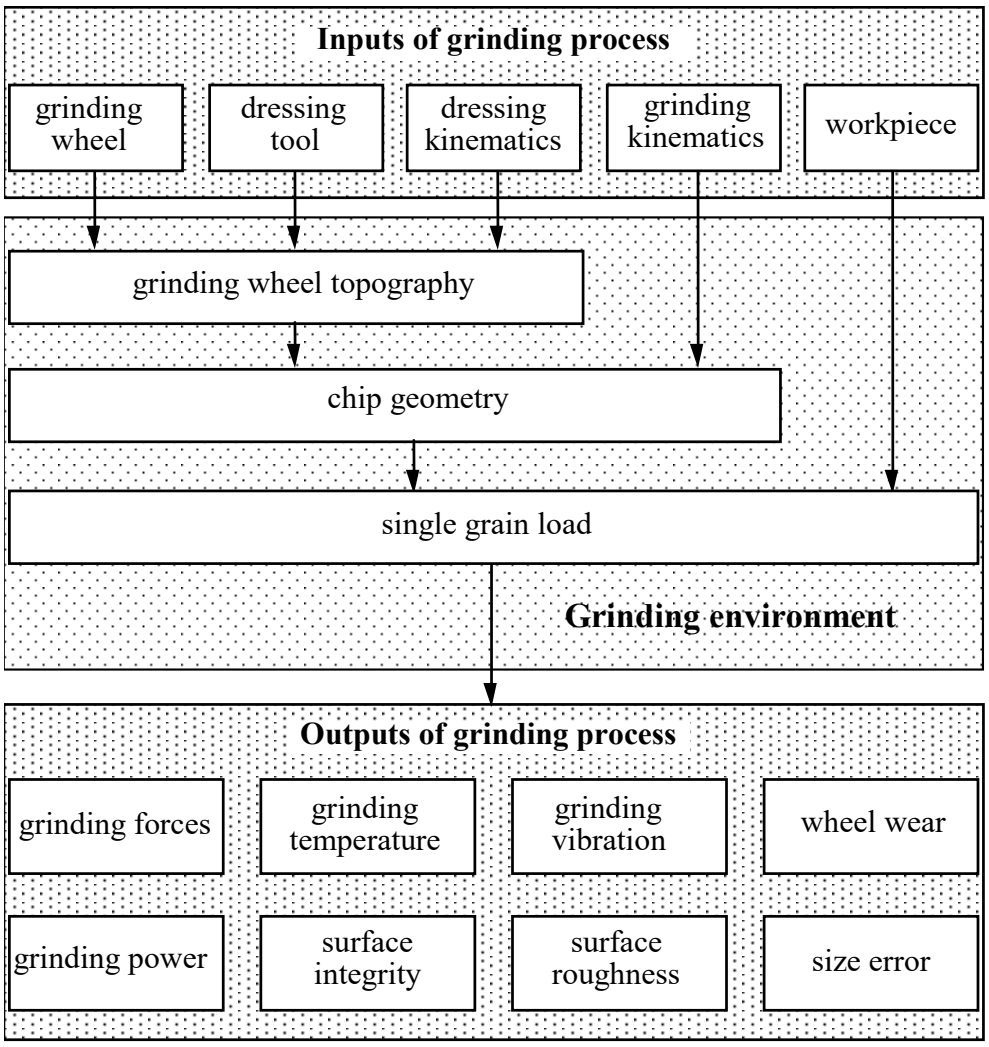

Fig. 1. A systematic view of inputs and outputs of a grinding process (Chen, & Rowe, 1996).

Material removal mechanism analysis with single grit grinding tests

In grinding process, the kinematic relationship between the grinding wheel and the workpiece motions applies all cutting grits on the wheel surface. Early studies of the grinding process were based on the mechanics of an average individual grit in the wheel surface (Guest, 1915; Alden, 1914). Some aspects of the grinding process by which a grit grinds can be illustrated by the geometrical relationship between the grit and the workpiece during a grinding process. The geometry of the undeformed chip is shown in Fig. 2. The undeformed chip shape is characterised by the cutting path length of the grit l_k and the maximum undeformed chip thickness h_m. Basic grinding control parameters such as depth of cut a, grinding speed v_s and work speed v_w are also illustrated in Fig. 2.

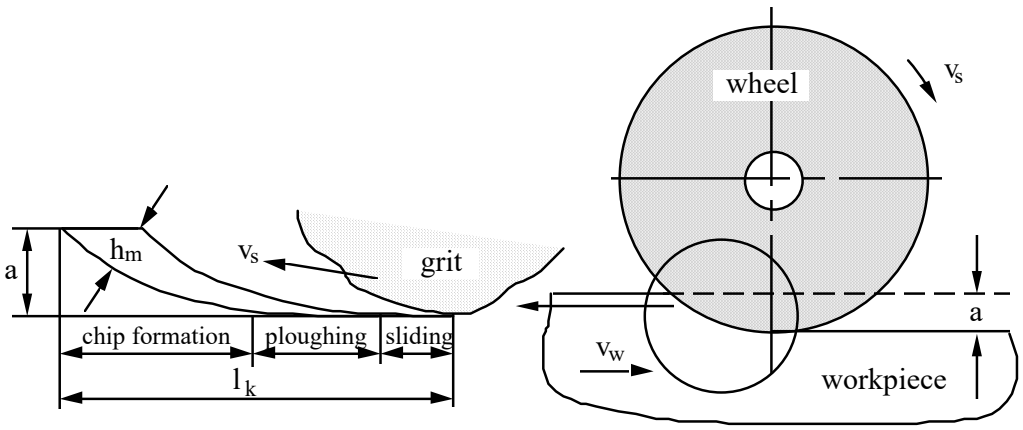

Fig. 2. Material removal mechanism in grinding (Chen, & Rowe, 1996).

Material removal mechanism at micro scale during grinding was first put forth by Hahn (1962). He proposed that the material removal in grinding consisted of three phases which were rubbing, ploughing and cutting. When the grit engages with the workpiece in an up-cut grinding, the grit initially slides without cutting on the workpiece surface due to the elastic deformation of the system. This is the rubbing phase. As the stress between the grain and workpiece is increased beyond the elastic limit, plastic deformation occurs. This is the ploughing phase, where the workpiece material piles up to the front and sides of the grit to form a groove. A chip is formed when the workpiece material can no longer withstand the tearing stress. The chip formation stage is the cutting phase. From the view point of the energy required to remove material, cutting is the most efficient phase. Rubbing and ploughing are inefficient, because the energy is wasted in deformation and friction with negligible contribution to material removal. Furthermore a high temperature may result in an excessive rate of wheel wear and the workpiece surface may suffer metallurgical damage (grinding burn). Therefore, rubbing and ploughing should be minimized because of the energy waste with adverse effects to the grinding performance.

In previous works, most of the investigations dealing with single grit-workpiece interaction were conducted by utilizing single grit scratch tests. Resultant scratches were analysed to understand the material removal mechanism. Albeit the majority of scratch tests was performed by using a shaped tool such as shaped-diamond grain (Transchel et al., 2013; Axinte, Butler-Smith, Akgun, & Kolluru,

2013), diamond indenter (Subhash, & Zhang, 2002; Gu, Yao, & Liang, 2011), diamond stylus (Komanduri, Varghese, & Chandrasekaran, 2010) at nanoscale, spherical tool (Anderson, Warkentin, & Bauer, 2011), or negative raked cutter (Barge, Rech, Hamdi, & Bergheau, 2008) to consider shape effects during material removal, some experimental works also exist with real abrasive grits (Matsuo, Toyoura, Oshima, & Ohbuchi, 1989; Brinksmeler, & Glwerzew, 2003; Nadolny, & Kapłonek, 2015; Öpöz, & Chen, 2015). The shaped tools (known geometry) have been preferred to obtain good agreement with computational model such as finite element models (Anderson et al. 2011; Doman, Warkentin, & Bauer, 2009; Doman, Bauer, & Warkentin, 2009). Besides, the shaped tools make parametric investigation easy to study the effect of speed, depth of cut, and hardness of materials on material removal mechanism by keeping the tool geometry stable. However, scratches with shaped tool diverge from the reality in actual grinding. In reality, the shape of the grit cutting edges continuously alters due to wear and fracture occur during grinding process (Öpöz, & Chen, 2012; Chen, & Öpöz, 2014). Therefore an investigation of material removal in grinding should also take account of grit shape changes during grinding process.

With a simple test rig setup on a Nanoform 250 machine as shown in Fig. 3, the material removal can be investigated by using a cubic boron nitride (CBN) grit to scratch workpiece as it acts in a grinding process. The grit size was around 0.5 mm in diameter and grit cutting speed v_c was 5.46 m/s (or spindle rotational speed n_s = 3000 rpm). The workpiece sample material was En24T steel (Element %: C 0.4, Si 0.23, Mn 0.58, Cr 1.2, Mo 0.28, Ni 1.5, S < 0.04, P < 0.03, Fe balance) with hardness of 289.2 HV at 1 kg measuring load. The trials were repeated several times by moving workpiece in the direction along wheel rotational axis. By raise one side of the sample slightly higher than the other side, the depth of cut of each scratch can be changed depending on its position. In this way, the different scratch marks can be created to present rubbing, plough and cutting phenomena at different depths of cut. Figure 4 shows a series of scratch passes of a grit on a workpiece sample under the same grinding condition, where the scratch cross section profiles changed due to the grit wear. The CBN grit initially produced single edge scratches in the test; then it created multiple edge scratches due to geometrical alteration of the grit cutting edges, which was caused by grit fracture, including micro cracking and attritious wear flat.

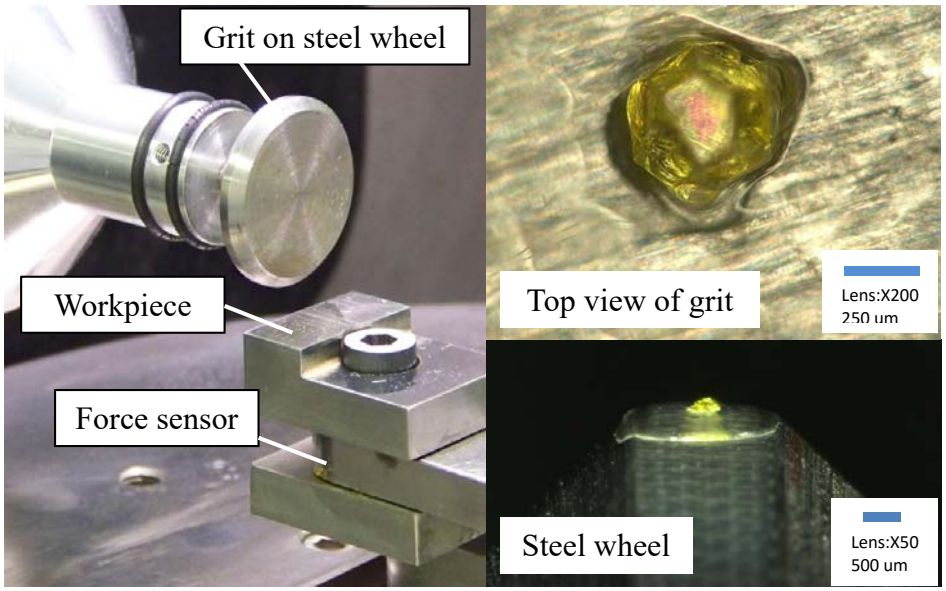

Fig. 3. Single grit grinding test setup

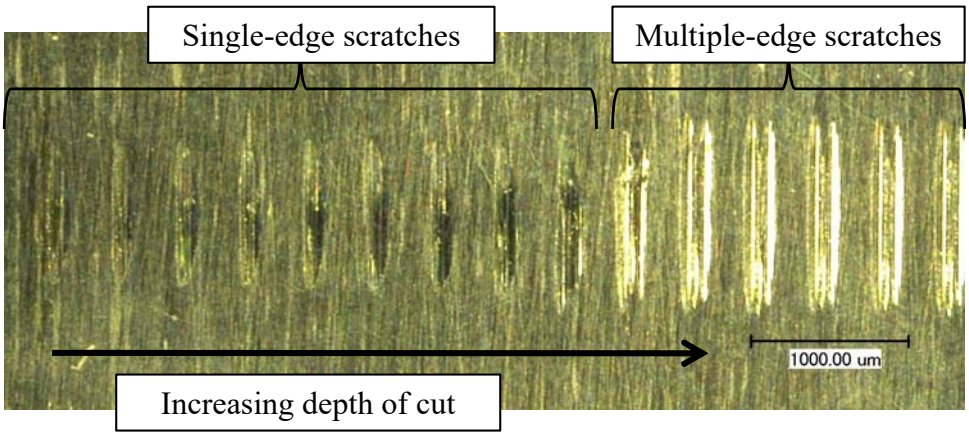

Fig. 4. Microscopic view of scratches with profile changes of cutting edge.

In order to examine the efficiency of material removal, the pile up ratio and actual material removal area should be considered. As shown in Fig. 5, the profile of cutting trace of grit paths was measured by using a Talysurf CCI 3000 white light interferometer. The pile up ratio is defined as the ratio of total ploughed materials piled up area (PA=green area) to total groove section area (GA=red area) in the cross section under the consideration, while the actual material removal area is determined by subtracting total pile up area from the groove cross section area (GA-PA). The actual material removal area is a measure to quantify material removal efficiency along the scratch profile. The pile up ratio and actual material removal area with respect to depth of cut are shown in Fig. 5. It is found that the pile up ratio is significantly higher with multiple cutting edge scratches than that with single cutting edge scratches. During multiple edges scratching, although each of cutting edges looks sharper, a large portion of pile-up materials makes the cutting inefficient. The grit with multiple cutting edges in fact acts blunter. This demonstrated that material removal with a grit that has only a single cutting edge could be more efficient than that with multiple sharp cutting edges. This finding explained the reason why bulky shape grits are preferable for grinding wheel manufacturers.

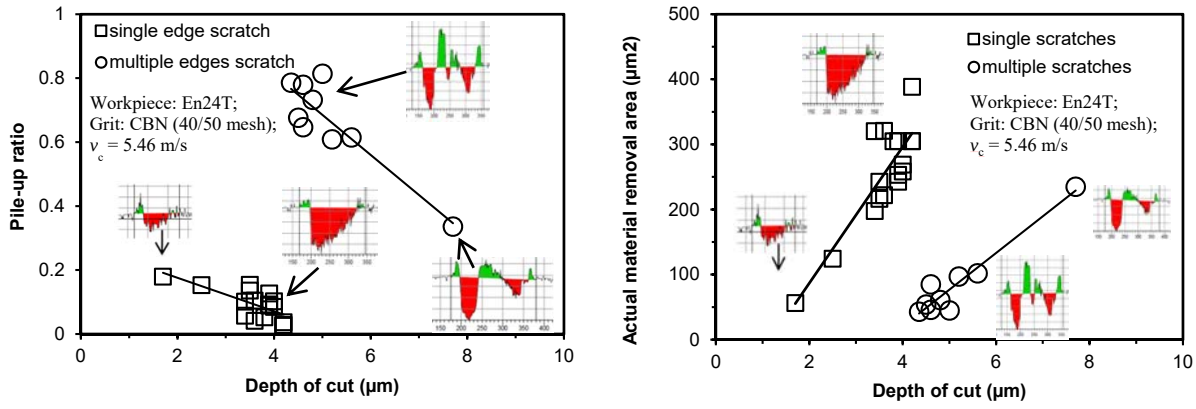

Fig. 5. Experimental results for single-edge and multiple-edges scratches

Acoustic emission in single grit grinding tests

The application of acoustic emission (AE) sensors has become very popular over last few decades. An AE signal can be defined as the transient elastic energy spontaneously released in materials undergoing deformation, fracture or combination of both (Dornfeld & Kannateyasibu, 1980). AE extraction has been used in many machining processes from milling, drilling to grinding where AE signals extracted from the material tests would traditionally use root-mean-squared (RMS) level, event count, energy distributions, amplitude and the powers of dominate frequency bands (Webster, Marinescu, & Bennett, 1994). The commonly used AE feature parameters for grinding AE are statistic parameters such as number of AE pulses, probability density of pulse amplitude, the peak of RMS values, crest factors analysis (i.e. the ratio of the peak to the RMS level of a signal), kurtosis, skew, autocorrelation, spectral density of AE and ratio of power at interested frequency ranges etc. (Aguiar, Serni, Dotto, & Bianchi, 2006; Chen, Griffin, & Liu, 2007; Han & Wu, 2013). Most researches on grinding AE monitoring directly link AE signals with grinding performance such as grinding force and grinding burn. The relation between the AE features and material removal mechanism are less understood.

The difference strength of acoustic emission (AE) can be observed in single grit scratching as illustrated in Fig. 6. The AE signals from single edge scratching are stronger than that from multiple cutting edges even though the depth of cut is smaller. As indicated in Fig. 5, the single cutting edge cutting is more efficient with less ploughing actions, the stronger AE signal amplitude in Fig. 6 may suggest that actual cutting actions generate stronger AE signal than the ploughing actions. Considering the relation between the AE strength and actual material removal area as shown in Fig. 7, it was noticed that AE signal strength actually tended to increase with the increase of actual material removal.

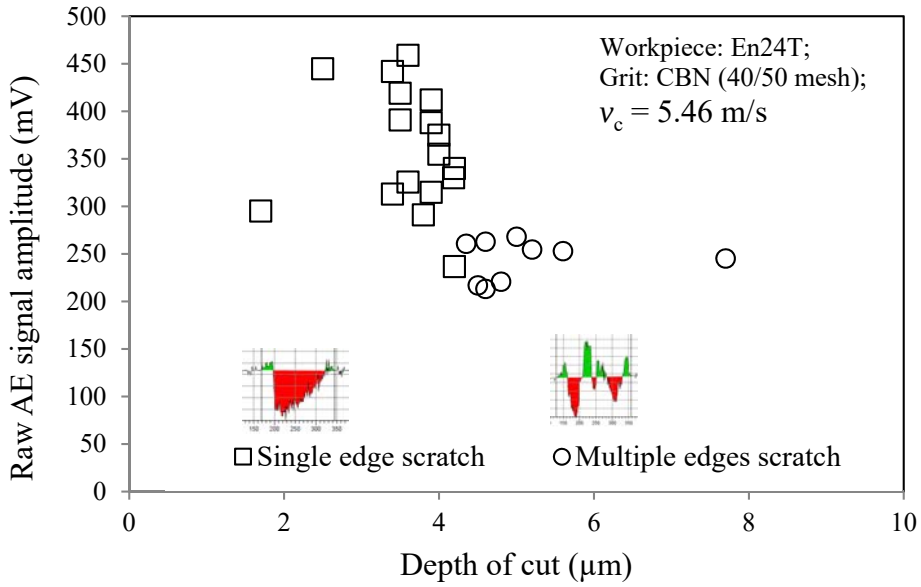

Fig. 6. Acoustic emission versus depth of cut in single grit grinding tests

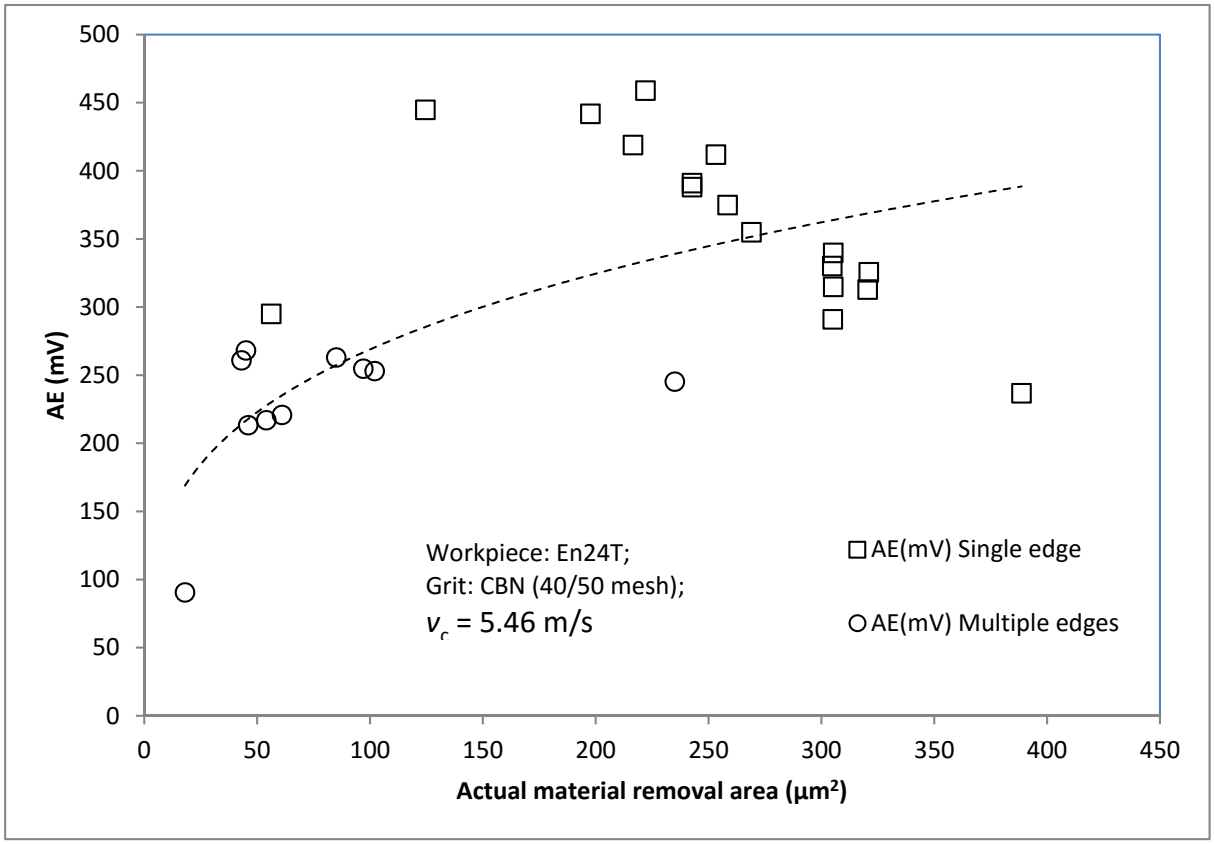

Figure 7. Acoustic emission versus actual material removal in single grit grinding tests

It is interesting to identify the features of grinding acoustic emission in relation to the rubbing, ploughing and cutting actions in single grit grinding. Figure 8 shows different AE power spectrums observed in single grit grinding. Figure 8(a) shows a rubbing situation where the grit passed workpiece surface without leaving any visible trace. It can be seen that rubbing AE power energy of concentrated in the range of less than 300 kHz. When grit actually ploughed and cut through workpiece, the AE signals presented broad band power spectrums whose frequency range were up to near 800 kHz. Considering the situation of similar material removal rate, i.e. the gouge cross section area is the same (about 55 µm^2), Fig. 8(b) and Fig. 8(c) show that multi-edge cutting presents higher AE energy in higher frequency range (>100 kHz); but the AE energy in the low frequency range is almost the same as single edge cutting. For similar scratch gouge depth (about 4.5 µm), Fig.8(c) and 8(d) show that single edge cutting gives higher AE energy amplitude in the low frequency range (<100 kHz) while multi-edge cutting present stronger AE elements in higher frequency range (>100 kHz). According to the observation discussed above, we may reasonably consider that the material removal or cutting action may be presented by the low frequency (<100 kHz) AE signals while the ploughing action may be presented by high frequency (>100 kHz) AE signals. It has also been noticed that multi-edge scratching presented more AE elements in the range between 600 ~ 800 kHz. As aforementioned fact that multiple edge scratch produced more ploughing actions, it could be reasonably argue that ploughing actions could generate AE signals with more higher-frequency elements than cutting actions.

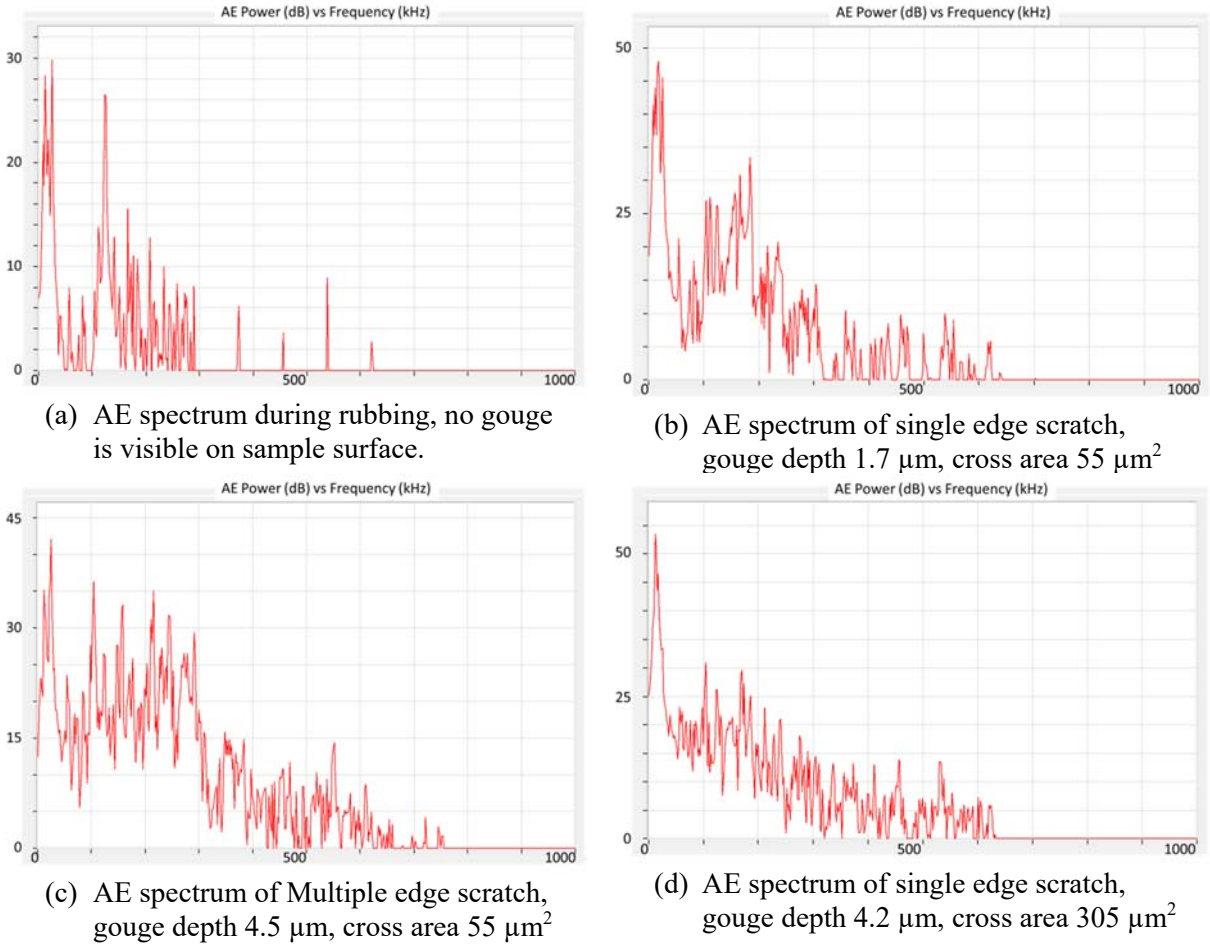

(a) AE spectrum during rubbing, no gouge is visible on sample surface.

(b) AE spectrum of single edge scratch, gouge depth 1.7 µm, cross area 55 µm^2

(c) AE spectrum of Multiple edge scratch, gouge depth 4.5 µm, cross area 55 µm^2

(d) AE spectrum of single edge scratch, gouge depth 4.2 µm, cross area 305 µm^2

Figure 8. AE spectrum in relation to different grinding mechanism.

Influence of dressing operation on the grinding behaviours

It has been demonstrated the influence of the shape of a grit on the material removal and related acoustic emission signals in the last section. As a cutting tool, the cutting surface condition of a grinding wheel is also determined by the wheel dressing operation. In general, the finer dressing conditions (small dressing depth and lead) will bring more cutting edges on the wheel surface [27]. As a misconceived opinion, the sharp cutting edges created by dressing process should provide effective cutting action leading to lower cutting force and finer surface. In fact, multiple sharp cutting edges on an abrasive grit are not necessarily leading to better cutting efficiency as illustrated in the last section.

The number of cutting edges on the wheel surface during grinding process will change towards an equilibrant status due to the wheel self-sharpening actions (Chen, Rowe, Allanson, & Mills, 1999). Umino and Shinozaki (1976) observed the variation of the cutting edge density $\lambda(t)$, which was expressed as

$$\lambda(t) = \lambda_e + (\lambda_0 - \lambda_e)\exp(-m\, n_s t) \quad (1)$$

where λ_0 is the initial cutting edge density after dressing. λ_e is the equilibrium cutting edge density after initial grinding wheel wear stage, m is the probability of grain fracture in one revolution of the

wheel, n_s is the wheel rotational speed and t is the wheel grinding time after dressing. The initial cutting edge density can be controlled by different dressing operation; the finer dressing applied, the higher the cutting edge density would be. However, the final equilibrium cutting edge density is determined by grit size, wheel structure, bonding strength and grinding strength. Normally, the larger grit size gives lower cutting edge density. By considering the effect of the initial changes in the number of cutting edges and the effect of attritious wear on the sharpness of wheel, the time dependent tangential grinding force was modelled (Chen et al. 1999) as

$$F_t = \left[k_2 + (k_1 a_d^{\alpha} f_d^{\beta} - k_2)\exp(-mn_s t)\right] b \left(\frac{v_s}{v_w}\right)^{1-\varepsilon} d_e^{1-\varepsilon} h_{eq}^{\varepsilon} + k_3 b n_s t \tag{2}$$

where k_1, k_2, k_3, α, β and ε are constants depending the process, a_d is dressing depth, f_d is dressing lead, b is grinding width, v_s is grinding speed, v_w is workspeed, d_e is equivalent grinding wheel diameter and h_{eq} is equivalent chip thickness. The equivalent grinding wheel diameter d_e is defined as

$$d_e = \frac{d_w d_s}{d_w + d_s} \tag{3}$$

where d_w is workpiece diameter and d_s is wheel diameter. The equivalent chip thickness h_{eq} is defined as

$$h_{eq} = \frac{a_e v_w}{v_s} \tag{4}$$

where a_e is the true depth of cut.

The Eq. (2) depicts grinding force can be influenced significantly by dressing condition right after dressing operation. After a certain period of grinding, the grinding force will converge to an equilibrant level depending on material removal strength and wheel wear condition. When the material removal rate is the same, i. e. the equivalent chip thickness h_{eq} is same, the lower grinding force or power indicates the grinding is more efficient in terms of grinding energy consumption. Our experimental results, Fig. 9, shows that the finer dressing condition is, the higher grinding power will be. This also confirms that higher cutting edge number created by finer dressing operation does not give higher cutting efficiency. From the results, it can be seen that the grinding power is initially high after dressing operation, but it will reduce to a certain level and then will increase again. Such a grinding behaviour is related to the wheel wear performance during grinding. The grinding operational conditions in Fig. 9 are grinding speed v_s = 33 m/s, workspeed v_w = 0.25 m/s, and the wheel infeed rate v_f = 10 μm/s, coolant is flushed into grinding zone.

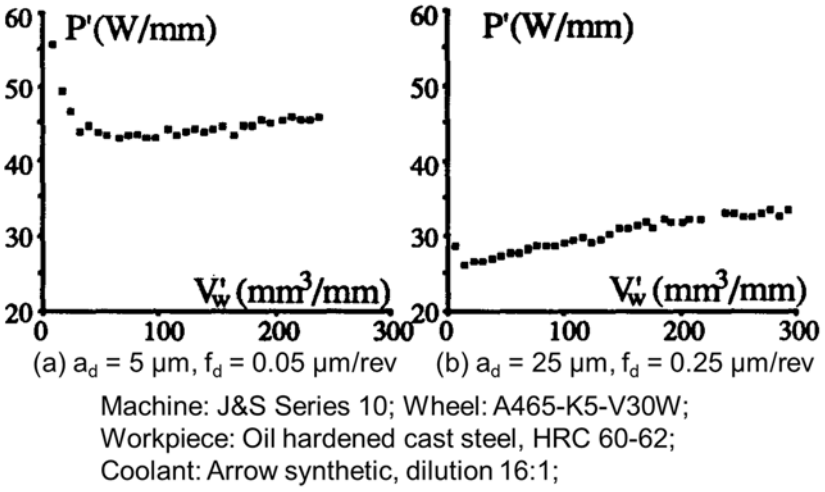

Fig. 9. Dressing effects on grinding power

Temperature elevation and thermal stresses in grinding zone

Energy consumed during grinding process will raise grinding zone temperature. Therefore, all influential factors on grinding force will in turn affect the thermal performance of grinding. The grinding zone temperature elevation is dependent on the grinding efficiency and the proportion of grinding energy that enters the workpiece. Experimental results (Rowe, Morgan, Black, & Mills, 1996) show that the energy transfer proportions between the workpiece and grinding wheel remain relatively constant; albeit the energy distribution is also affected by the coolant supply.

The thermal energy transfer in grinding can be simplified as a band of heat passing a semi-infinite workpiece body at a workspeed v_w. The solution of the temperature distribution for this problem involves modified Bessel functions. For a uniform heat source, the temperature distribution under the workpiece surface can be expressed as (Carslaw & Jaeger, 1959)

$$T = \frac{2}{\sqrt{\pi}} \frac{R_w q \sqrt{t_c}}{\sqrt{k_w \rho_w c_w}} \exp\left(\frac{-z^2}{4Kt_c}\right) - \frac{qz}{k_w}\left(1 - \operatorname{erf}\frac{z}{2\sqrt{Kt_c}}\right) \quad (5)$$

where R_w is the partition ratio of the heat flux into the workpiece to the total heat flux q in the grinding zone, z is the depth from the workpiece surface, t_c is the time the heat source acts on a point at the workpiece surface, k_w is the workpiece thermal conductivity, ρ_w the workpiece density and c_w is the specific heat capacity of the workpiece. The thermal diffusivity of the workpiece K is equal to $k_w/\rho_w c_w$. For the calculation of maximum grinding surface temperature, t_c is equal to the time that the wheel takes to pass over the grinding zone, therefore $t_c = l_e/v_w$, where l_e the real grinding contact length. Hahn (1962), Black (1996), Rowe, Black, Mills, Morgan, & Qi (1997) noticed that contact condition between grit and workpiece has significant influence on the heat partition ratio, which should be considered in grinding temperature models. Zhu, Li and Ding (2013) experimentally demonstrated the sharp grit gave lower temperature and improved energy partition ratio model by taking grit shape into account.

The temperature distribution is found to be strongly affected by the heat source distribution and Peclet number, which is defined as $v_w\, l/2K$, where l is half the heat source length. For most conventional grinding operations the Peclet number is higher than 5. In such cases, the difference of maximum

temperature elevation between uniform and triangular heat sources is around 6% under the one-dimensional analysis assumption (Chen, Rowe, & McCormack, 2000).

The temperature elevation during grinding leads to a material expansion of the workpiece surface. Because the bulk of the workpiece material under the surface is still cool, the surface thermal expansion is constrained. As the consequence, the surface expansion produces compressive stress in the surface layer of the workpiece. The value of the thermal stress depends on the temperature gradient and the material elastic modulus.

When the thermal stress value reaches the yield stress of the material, plastic deformation occurs in the workpiece surface. This leaves permanent deformation in the workpiece surface. As the material cools, tensile stresses are created and remain in the ground surface. The material yield stress is usually a function of temperature. As indicated in Eq. (5), the temperature of the workpiece varies with the depth (z-direction) under the workpiece surface. Therefore the elastic stresses along the x and y directions are assumed to be the same and are functions of depth z. Considering the situation that the thermal stress is smaller than the material yield point, the thermal stress can be determined from elastic stress analysis (Chen et al., 2000; Johns, 1965).

$$\sigma(z) = \frac{1}{1-\nu}[-E\alpha T + \frac{1}{d}\int_{-d/2}^{d/2} E\alpha T dz + \frac{12z}{d^3}\int_{-d/2}^{d/2} E\alpha T z dz] \quad (6)$$

where ν the material Poisson ratio, E the elastic modulus, α the coefficient of thermal expansion, d the thickness of the workpiece and T the temperature distribution at the time when the grinding surface temperature reaches its maximum. The temperature distribution can be calculated by using Eq. (5). The stresses determined from Eq. (6) can be used to determine the strains if required. When the surface grinding temperature reaches its maximum, the thermal stress on the workpiece surface also reaches a maximum. If the thermal stress is lower than the material yield stress, no residual stress will be introduced owing to thermal effects.

Grinding performance monitoring using thermal acoustic emission in grinding

As the aforementioned, grinding material removal process generally involves rubbing, ploughing and cutting three stages in a grit cutting pass. Such a process induces a significant mechanical stresses including elastic deformation and plastic shear stresses. The rubbing and ploughing contribute little to material removal, while the cutting or chip formation is the desirable grinding function that removes materials. All these functions would create heat that elevates grinding temperature. Often, the grinding heat generation or temperature elevation can also be a measure the grinding efficiency. For the same material removal rate, the lower temperature elevation means the better grinding efficiency.

As indicated in Eq. (5), grinding temperature is a function of grinding power. Therefore monitoring grinding power can also indicate the grinding performance. Due to the grinding power signal is normally extracted from grinding wheel spindle, it may not be sensitive enough to show the fast changes of grinding performance. For example, under the same grinding condition, Fig. 10 shows that grinding power is relatively insensitive to the fast changes of grinding performance while grinding acoustic emission (AE) signal can detect grinding cycle start point much earlier (0.25 seconds in this case) and can illustrate grinding performance changes in every work revolution. To this end, grinding acoustic emission is a better option for grinding process monitoring.

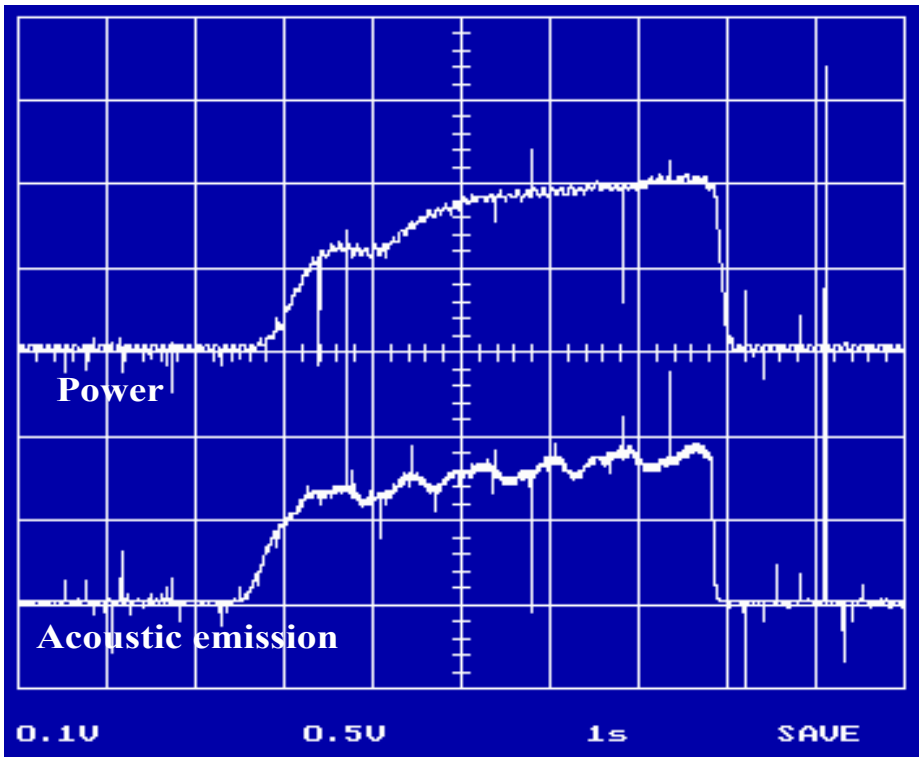

Figure 10. Comparison of grinding power signals and grinding acoustic emission signals

As the grinding temperature arises, it induces thermal stress, which could excite material atoms or molecules to release acoustic waves. Such acoustic emission will contain some physical attributes of materials at different temperatures. This led a novel way for temperature monitoring (Chen, Mohamed, & Folkes, 2012). By monitoring the thermal acoustic emission, the grinding efficiency can be judged in relation to grinding thermal behaviour. To achieve this, the key issue of the thermal acoustic emission monitoring method is to identify the thermal AE signatures in relation to different grinding temperature without involving any mechanically induced stresses. A laser irradiation simulation of grinding temperature elevation is a critical technique. Fig. 11 shows a test rig setup on Lumonics JK704 laser machine for thermal AE signature identification. The laser irradiation density can be controlled by adjusting the offset focal distance. By carefully selecting laser irradiation conditions, the temperature elevation under laser irradiation can be the same as that in grinding. Fig. 12 shows that similar temperature elevation features in a laser test and a grinding trial. This means that creation of grinding thermal stress may be simulated by laser irradiation. Liu, Chen, & Gindy, (2006) made a comparison of AE spectrum under low and high temperatures and convinced that the thermally induced acoustic emission has different responsive AE features from mechanically induced acoustic emission. This provides a useful clue for the application of AE detection technique for grinding temperature monitoring.

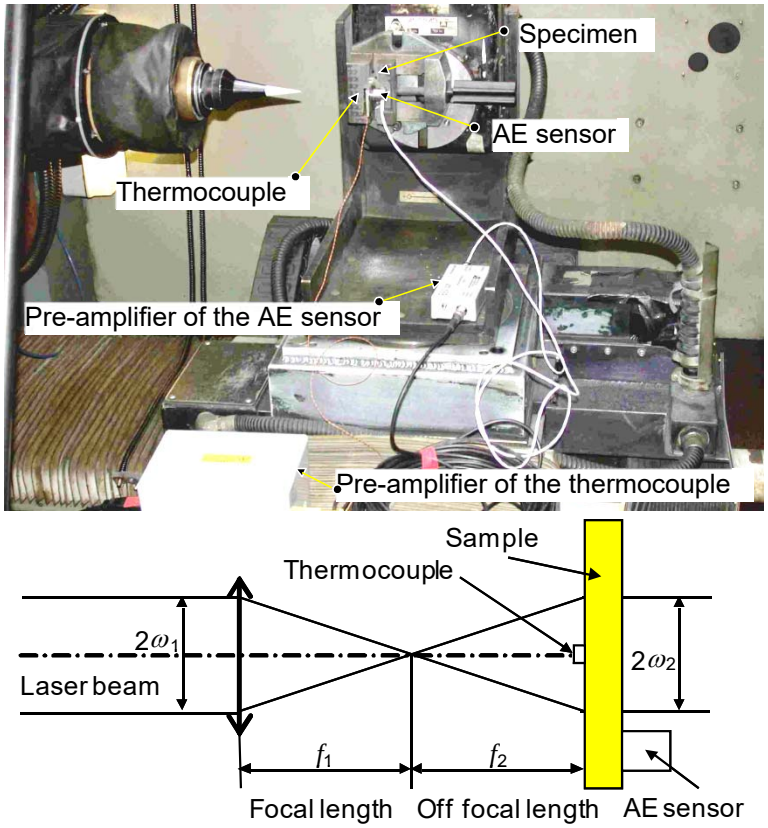

Fig. 11. Laser irradiation setup for thermal AE signature identification

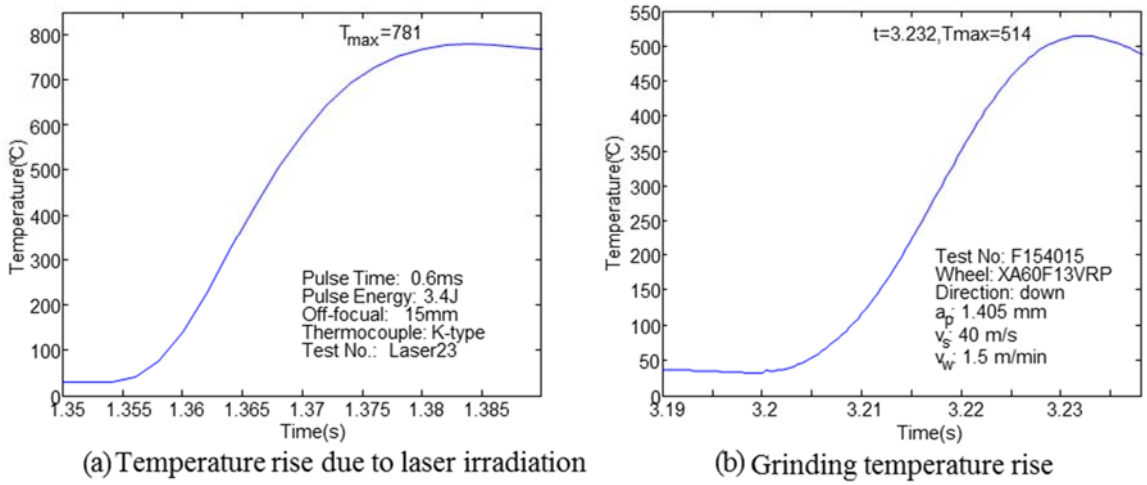

(a) Temperature rise due to laser irradiation (b) Grinding temperature rise

Figure 12. Temperature elevation during laser irradiation and grinding

Fig. 13 shows the surface temperature elevations under laser irradiation with different off focal lengths. The smaller off focal length means higher laser power intensity, which leads to high surface temperature. The thermally induced AE signals and spectrums illustrate significant difference at different temperature in terms of the AE signal amplitude and feature frequency range as shown in Fig.

14. It can be seen that higher temperature (shorter off focal length) will create higher AE signals amplitude and stronger spectrum elements in high frequency ranges. Therefore it is rational to use AE signal features to interpret the level of temperature elevation.

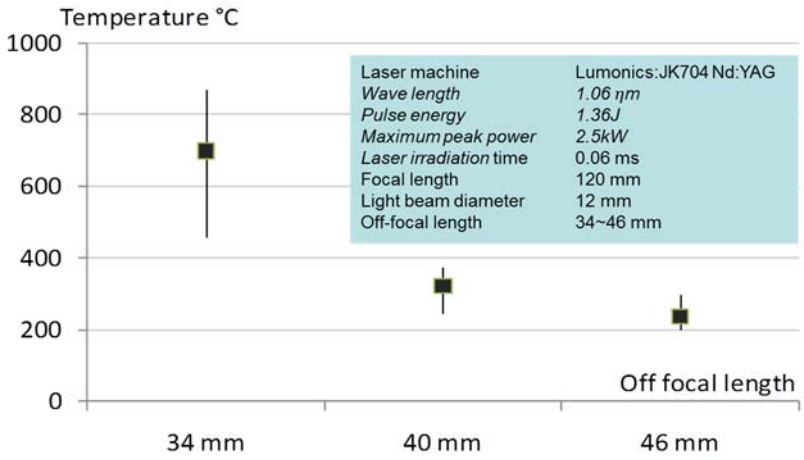

Fig. 13. Temperature elevation due to laser irradiation

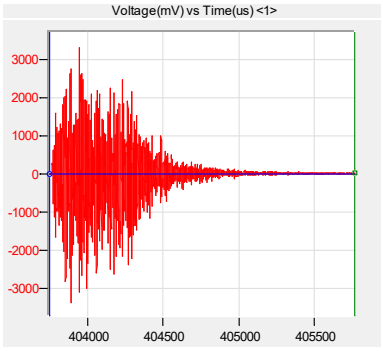

(a) AE signal created by laser with off-focal length 34 mm

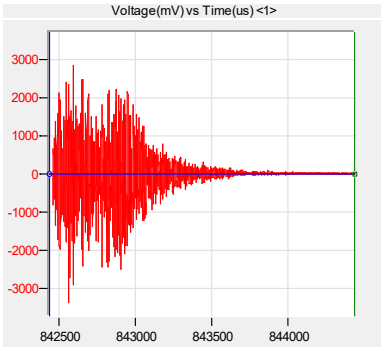

(b) AE signal created by laser with off-focal length 40 mm

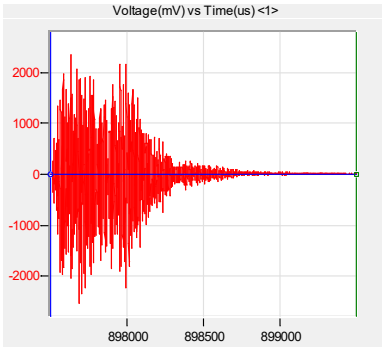

(c) AE signal created by laser with off-focal length 46 mm

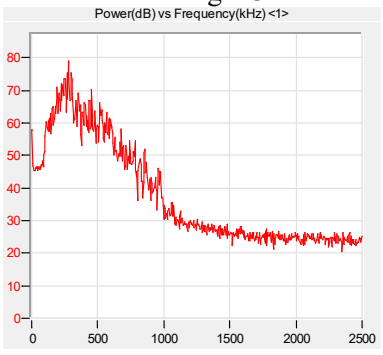

(d) AE spectrum for the case of laser off-focal length 34 mm

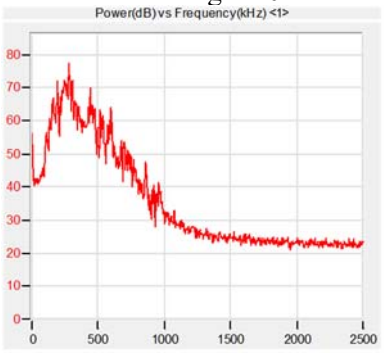

(e) AE spectrum for the case of laser off-focal length 40 mm

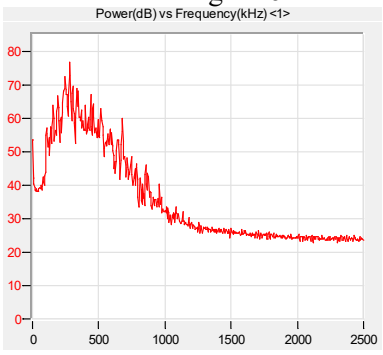

(f) AE spectrum for the case of laser off-focal length 46 mm

Figure 14. The AE spectrum under different temperature elevation conditions

The common signal processing methods to interpret the AE signal features are aforementioned statistic methods, which require a lot human efforts to make subjective interpretation based on experience. In order to objectively extract meaningful AE signal features that might represent the temperature elevation, an artificial neural network (ANN) may be a right tool to use. The neural network tool has been used since the 1960s (Duda, Hart, & Stork, 2001). The advantages of neural networks over pattern recognition are that it can easily constitute optimum nonlinear multi-input functions for pattern recognition and the accuracy of pattern recognition is easily improved by learning processes. Through a series of researches, a back propagation neural network has been applied to classify high, medium and low temperatures in relation to laser irradiation arrangement. The ANN was constructed using Matlab Neural Network Toolbox with 6 hidden layers with 256 elements in the input layer. The log sigmoid function is used as transfer function in the hidden layers. Learning rate is $1x10^{-9}$. During the ANN training process, the short time Fourier transformation (STFT) of AE signals from laser irradiation tests were used as inputs with the outputs being high, medium and low temperatures. Once the network architecture has been defined, the network can be created and optimised according to its error function.

The training data set consisted of thermal AE data which were extracted from the laser irradiation tests. The input data consists of AE data extracted from 34mm, 40mm and 46mm off-focal distances which are concatenated together as training inputs. The target vector in relation to the network was defined in such a way that the high temperature was assigned a value of 3, medium temperature was assigned a value of 2 and the low temperature was assigned a value of 1. The outputs of the trained network represented each case correctly as shown in Fig. 15, where the straight horizontal line is defined target value and the circles are actual ANN outputs from training data. The results are completely satisfactory, which means the ANN can extract the AE features that represent different temperature elevations.

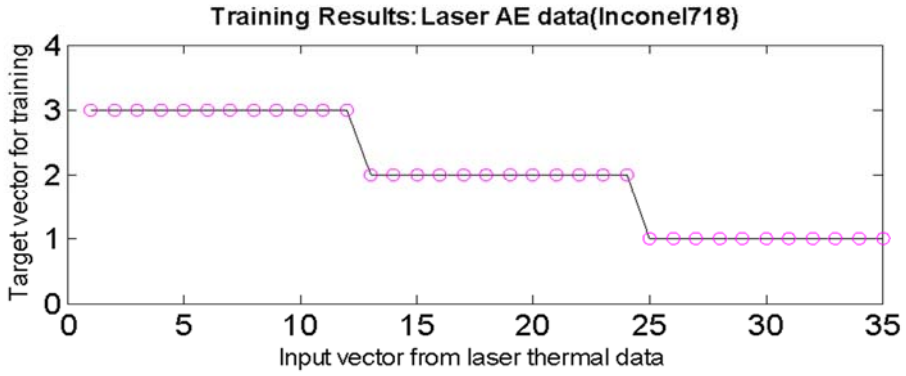

Figure 15. The learnt training set for an ANN classification system.

Once the neural network has been trained by laser thermal AE data, it becomes a classifier to identify different material behaviours under different temperature elevation. Therefore the trained ANN can be applied for grinding monitoring using the AE data extracted from grinding experiments. Six grinding trials were arranged on Makino A55 machine centre. An Inconel 718 (Element %: Ni 53, Cr 19, Mo 31, Nb 5.1, Co 1.0, Mn 0.35, Cu 0.5, Al 0.9, Ti 0.3, Si 0.35, C 0.08, S 0.015, P 0.015, B 0.006, Fe balance) sample was ground with 0.02 mm of depth of cut, 1 m/min of workspeed and 55 m/s of

grinding speed in a sequential manner. The wheel was dressed only once just before the trials. Thirty sets of AE feature data were extracted from each grinding test using STFT technique. By using the trained ANN, the proportions of different thermal AE features that represent different temperature levels in the tests are listed in Table 1.

Table 1: Classification of temperature elevation in Inconel 718 grinding at 0.02 mm depth of cut

Material :Inconel 718	**cut1**	**cut2**	**cut3**	**cut4**	**cut5**	**cut6**
Depth of cut: 0.02 mm	30 set	30 set	30 set	30 set	30 set	30 set
ANN output value = 3	3.33%	0	0	0	0	13.33%
ANN output value = 2	60.66%	70%	30%	56.66%	50%	83.33%
ANN output value = 1	30%	30%	70%	43.34%	50%	3.33%
ANN output value: 1 – low temperature; 2 – medium teperature; 3 – high temperature						
Grinding conditions	Grinder: Makino A55 Grinding wheel: XA60F VRP Materials: Inconel 718			Depth of cut: 0.02 mm, Workspeed: 1 m/min, Grinding speed 55 m/s.		
Inconel 718 composition (Element: %)	Ni 53, Cr 19, Mo 31, Nb 5.1, Co 1.0, Mn 0.35, Cu 0.5, Al 0.9, Ti 0.3, Si 0.35, C 0.08, S 0.015, P 0.015, B 0.006, Fe balance					

Due to the random nature of grit positions on the wheel surface, the instant grinding temperature in relation to individual grit may vary significantly. Therefore the AE signals in each moment in the grinding trials may present different proportion of thermal features that represent different temperatures. Such information is particularly useful for grinding wheel wear monitoring. Looking at Table 1, it can be seen that 60.66% AE data are classified as medium temperature and 30% AE data are classified as low temperature in the first cut. Only minute AE signals (3.33%) illustrated high temperature features. This may relate to initial dressing effects, since some multi-edge grits right after wheel dressing may act bluntly as discussed previously. After initial wheel wear stage, these blunt grits may dislodge and the wheel surface will settle in a stable sharp status as it can be seen in the test cut 2. The newly dressed wheel wears quickly as the defects created during dressing operation will drop out quickly leaving sharp grits on the wheel surface. As grinding continues, the wheel will keeping its sharpness because the self-sharpening ability. The grinding temperature will keep low until the wheel reach its life as shown in cut 6, where the proportion of high temperature increases. Such a grinding performance in a wheel dressing cycle is the same as what has been discussed on the effects of dressing on grinding power. From this example, it can be concluded that grinding performance can be monitored by using the thermal AE features identified from laser irradiation tests. By applying this method, grinding monitoring could be much easier and cheaper, because grinding trials can be eliminated for ANN training, which often be considered as most expensive activity in process monitoring. It is worthwhile to mentioning that application ANN for grinding problem monitoring is not scarce, but it needs significant effort in training a suitable ANN that varies on case by case scenario. The new method can significantly reduce the efforts spent on the ANN training.

Conclusive remarks

With the researches presented in this paper, following conclusions could be summarised.

By reviewing the fundamentals of grinding process, the material removal with each abrasive grain on grinding wheel surface is the core of grinding. During grinding, rubbing and ploughing are not efficient in terms of material removal, only cutting action is ideal. It has demonstrated that multiple sharp cutting edges on an abrasive grit in a grinding wheel surface do not necessarily provide higher cutting efficiency, because they also introduce more ploughing actions. Although a finer dressing can lead better ground surface finish, it also leads to higher power consumption and higher grinding temperature. This is due to more cutting edges created after a finer dressing operation.

In this paper, it has demonstrated that acoustic emission is more sensitive to the variation of grinding performance than grinding power. It also shows that the action of grit rubbing could generate AE signals of frequency range up to 300 kHz, while AE signals from ploughing and cutting actions have broader frequency up to 800 kHz. Furthermore, the ploughing action could excite more high frequency AE signals.

Due to the quick temperature elevation in grinding, thermal induced stresses in grinding zone are significant and will trigger acoustic emission. By use laser irradiation on a workpiece surface, the elevation of grinding temperature was simulated, where thermal induced AE signals have even wider frequency band (up to 1 MHz of the sensor frequency responding range). Such thermal induced acoustic emission has rich information to present material performance under different temperatures, which also represented the changes of grinding wheel surface condition in the grinding process. Therefore it can be used for grinding process monitoring. In this paper, a novel AE monitoring method is introduced and it has demonstrated potential application in monitoring grinding wheel wear situation and grinding efficiency.

In a ward, the AE signals possess rich information that responds the changes in grinding quickly and precisely in relation to fundamental material removal phenomena. The knowledge identified regarding the relation between grinding physical performance and AE signals provide great insight of grinding for engineers to improve grinding efficiency through online monitoring and control. How to interpret the AE signals intelligently in relation to various grinding behaviours is still a remaining task for scientists to explore.

Reference

Aguiar, P. R., Serni, P. J. A., Dotto, F. R. L., Bianchi, E. C., (2006). In-process grinding monitoring through acoustic emission, *J. Braz. Soc. Mech. Sci. & Eng*., 28(1), 118-124

Alden, G. I., (1914). Operation of Grinding Wheels in Machine Grinding. *ASME Trans*., 36, 451-460.

Anderson, D., Warkentin, A., & Bauer, R. (2011). Experimental and numerical investigations of single abrasive-grain cutting. *International Journal of Machine Tools and Manufacture*, 51(12), 898-910.

Axinte, D., Butler-Smith, P., Akgun, C., & Kolluru, K. (2013). On the influence of single grit micro-geometry on grinding behavior of ductile and brittle materials. *International Journal of Machine Tools & Manufacture*, 74, pp. 12-18.

Barge, M., Rech, J., Hamdi, H., & Bergheau, J.M. (2008). Experimental study of abrasive process. *Wear*, 264(5-6), 382-388.

Batako, A. D. L. and Goh, S. Y. (2014). Workpiece roundness profile in the frequency domain: an application in cylindrical plunge grinding. *Int J Adv Manuf Technol*, 72, 277–288.

Black, S. C. E. (1996). *The effect of abrasive properties on the surface integrity of ground ferrous components*. PhD Thesis, Liverpool John Moores University.

Brinksmeler, E., & Glwerzew, A. (2003). Chip formation mechanisms in grinding at low speeds. *CIRP Annals-Manufacturing Technology*, 52 (1) 253-258.

Carslaw, S., & Jaeger, J. C. (1959). *Conduction of Heat in Solids*, Oxford University Press, London.

Chen, X. (2009). Machining Dynamics in Grinding Processes. *Chapter 8 in the book: Machining Dynamics: Fundamentals*, Applications and Practices, Kai Cheng (Ed), Springer,

Chen, X., & Öpöz, T. T. (2014). Characteristics of material removal processes in single and multiple cutting edge scratches. *International Journal of Abrasive Technology*, 6(3), 226-242.

Chen, X., & Rowe, W. B., (1996). "Analysis and simulation of the grinding process. Part II. Mechanics of grinding. *International Journal of Machine Tools and Manufacture*, 36 (8), 883–896.

Chen, X., Griffin, J., & Liu, Q. (2007). Mechanical and thermal behaviours of grinding acoustic emission. *International Journal of Manufacturing Technology and Management*, 12(1-3), 184-199.

Chen, X., Griffin, J., Liu, Q., Mechanical and thermal behaviours of grinding acoustic emission. *International Journal of Manufacturing Technology and Management*, 2007, 12 (1-3), 184-199.

Chen, X., Mohamed, A., & Folkes, J. (2012). Grinding Monitoring through Thermal Acoustic Emission Signatures. *Advanced Materials Research*, 325, 287-293.

Chen, X., Rowe, W. B., & Cai, R. (2002). Precision grinding using CBN wheels. *International Journal of Machine Tools & Manufacture*, 42 (5), 585–593.

Chen, X., Rowe, W. B., & McCormack, D. F. (2000). Analysis of the Transitional Temperature for Tensile Residual Stress in Grinding. *Journal of Materials Processing Technology*, 107(1), 216-221.

Chen, X., Rowe, W. B., Allanson, D. R., & Mills, B. (1999). A Grinding Power Model for Selection of Dressing and Grinding Conditions. *The Journal of Manufacturing Science and Engineering, Transactions of ASME*, 121(4), 632-637.

Comley, P., Walton, I., Jin, T., & Stephenson, D.J. (2006). A High Material Removal Rate Grinding Process for the Production of Automotive Crankshafts. *CIRP Annals - Manufacturing Technology*, 55(1), 347-350.

Doman, D.A., Bauer, R., & Warkentin, A. (2009). Experimentally validated finite element model of the rubbing and ploughing phases in scratch tests. *Proceedings of the Institution of Mechanical Engineers, Part B: Journal of Engineering Manufacture*, 223(12), 1519-1527.

Doman, D.A., Warkentin, A., & Bauer, R. (2009). Finite element modeling approaches in grinding. *International Journal of Machine Tools and Manufacture*, 49(2), 109-116.

Dornfeld, D. A., & Kannateyasibu, E. (1980). Acoustic Emission During Orthogonal Metal Cutting. *International Journal of Mechanical Sciences*, 22(5), 285-296.

Duda, R. O., Hart, P. E., & Stork,D. G. (2001). *Pattern Classification*, 2nd Edition, John Wiely & Sons, INC.

Griffin, J. and Chen, X. (2014). Real-time fuzzy-clustering and CART rules classification of the characteristics of emitted acoustic emission during horizontal single-grit scratch tests. *The International Journal of Advanced Manufacturing Technology*, 74(1), 481-502.

Gu, W., Yao, Z., & Liang, X. (2011). Material removal of optical glass BK7 during single and double scratch tests. *Wear*, 270(3-4), 241-246.

Guest, J. J. (1915). *Grinding Machinery*, Edward Arnold, London.

Hahn, R.S. (1962). On the nature of the grinding process. *Proceedings of the 3rd International Machine Tool Design & Research Conference*, Manchester, pp. 129-154.

Han, X. and Wu, T. (2013). Analysis of acoustic emission in precision and high-efficiency grinding technology. *Int J Adv Manuf Technol*, 67, 1997–2006.

Johns, D.J. (1965). *Thermal Stress Analyses*, Pergamon Press, Oxford.

Komanduri, R., Varghese, S., & Chandrasekaran, N., (2010). On the mechanism of material removal at the nanoscale by cutting. *Wear*, 269(3-4), 224-228.

Liu, Q., Chen, X., & Gindy, N. (2006). Investigation of acoustic emission signals under a simulative environment of grinding burn. *International Journal of Machine Tools & Manufacture*, 46(3-4), 284-292.

Matsuo, T., Toyoura, S., Oshima, E., & Ohbuchi, Y. (1989). Effect of grain shape on cutting force in superabrasive single-grit tests. *CIRP Annals, Manufacturing Technology*, 38 (1), 323-326.

Nadolny, K., & Kapłonek, W. (2015). Analysis of the effects of the single abrasive-grain microcutting scratch on INCOLOY Alloy 800HT by using advanced CLSM-SEM techniques. *Proc IMechE Part J: Journal of Engineering Tribology*, 229(6), 733-745.

Öpöz, T. T., & Chen, X. (2012). Experimental investigation of material removal mechanism in single grit grinding. *International Journal of Machine Tools & Manufacture*, 63(12), 32–40.

Öpöz, T. T., & Chen, X. (2015). Experimental study on single grit grinding of Inconel 718. *Proc IMechE Part B: Journal of Engineering Manufacture*, 229(5), 713-726.

Rowe, W. B. (2009). *Principles of modern grinding technology*, Norwich, NY: William Andrew.

Rowe, W. B., Black, S. C. E., Mills, B., Morgan, M. N., & Qi, H. S. (1997). Grinding temperatures and energy partitioning. *Proc: Math, Phys Eng Sci*, 453(1960): 1083–1104.

Rowe, W. B., Morgan, M. N., Black, S. C. E., & Mills, B., (1996). A simplified approach to control of thermal damage in grinding. *Annals of CIRP*, 45(1), 299-302.

Subhash, G., & Zhang, W. (2002). Investigation of the overall friction coefficient in single-pass scratch test. *Wear*, 252(1), 123-134.

Transchel, R., Heini, F., Stirnimann, J., Kuster, F., Leinenbach, C., & Wegener, K. (2013). Influence of the clearance angle on the cutting efficiency of blunt, octahedral-shaped diamonds in an active filler alloy. *International Journal of Machine Tools & Manufacture*, 75, 9-15.

Umino, K . & Shinozaki, N. (1976). One Aspect of Variation of Grinding Wheel Surface Based on Grinding Force Analysis: Studies on Wear and Redress Life of Grinding Wheel (1st report). *Semishu Kikai*, 42(4), 299-305.

Webster, J., Marinescu, I., & Bennett, R. (1994). Acoustic emission for process control and monitoring of surface integrity during grinding. *Ann CIRP*, 43(1):299–304.

Zhou, H. (2010). High-Efficiency and Ultraprecision Grinding of Soft-Brittle CdZnTe Crystals. *Materials and Manufacturing Processes*, 25, 418–423.

Zhu, D., Li, B., Ding, H. (2013). An improved grinding temperature model considering grain geometry and distribution. *Int J Adv Manuf Technol*, v. 67:1393–1406.